Ultrashort echo time (UTE) imaging using gradient pre-equalization and compressed sensing

CrossMark

Hilary T. Fabich *, Martin Benning, Andrew J. Sederman, Daniel J. Holland

Department of Chemical Engineering and Biotechnology, University of Cambridge, New Museums Site, Pembroke Street, Cambridge CB2 3RA, United Kingdom

ABSTRACT

Ultrashort echo time (UTE) imaging is a well-known technique used in medical MRI, however, the implementation of the sequence remains non-trivial. This paper introduces UTE for non-medical applications and outlines a method for the implementation of UTE to enable accurate slice selection and short acquisition times. Slice selection in UTE requires fast, accurate switching of the gradient and r.f. pulses. Here a gradient "pre-equalization" technique is used to optimize the gradient switching and achieve an effective echo time of 10 μs. In order to minimize the echo time, k-space is sampled radially. A compressed sensing approach is used to minimize the total acquisition time. Using the corrections for slice selection and acquisition along with novel image reconstruction techniques, UTE is shown to be a viable method to study samples of cork and rubber with a shorter signal lifetime than can typically be measured. Further, the compressed sensing image reconstruction algorithm is shown to provide accurate images of the samples with as little as 12.5% of the full k-space data set, potentially permitting real time imaging of short T_2^* materials.

© 2014 The Authors. Published by Elsevier Inc. This is an open access article under the CC BY license (http://creativecommons.org/licenses/by/3.0/).

1. Introduction

Ultrashort echo time (UTE) [1] imaging is a valuable technique for imaging short T_2 and T_2^* samples, however, its implementation is challenging and acquisition times can be long. Although the UTE pulse sequence is simple in theory, successful implementation requires accurate timing and a detailed understanding of the hardware performance [2]. This paper outlines a method to implement and optimize UTE to achieve accurate slice selection. The pulse sequence is also combined with compressed sensing (CS) [3] to reduce the acquisition time and potentially enable the study of dynamic systems.

UTE imaging was introduced to enable imaging of tissues in the body with short T_2 materials [1]. UTE has been used to study cartilage, cortical bone, tendons, knee meniscus and other rigid materials that would produce little or no signal from conventional imaging techniques [4–8]. However, few studies have been shown outside of medical imaging, despite widespread interest in short T_2 and T_2^* materials.

Many materials of interest in science or engineering applications will present short T_2 and T_2^* relaxation times due to

heterogeneity. These systems could include chemical reactors, plants in soil, shale rock, or polymeric materials. In a polymer network the T_2^* can range from the order of 10 μs to 1 ms depending on the rigidity of the network [9]. The other systems present similarly short relaxation times. Thus, UTE will open new possibilities for studying a range of materials outside of the medical field.

Chemical reactors, such as fluidized beds [10,11], are particularly challenging to study as they are dynamic and thus require short acquisition times. Techniques such as Echo Planar Imaging (EPI) and Rapid Acquisition with Relaxation Enhancement (RARE) are fast but not well suited to materials with short relaxation times. Fast Low Angle Shot (FLASH) is a gradient echo technique and can be used for rapid imaging of relatively short T_2 material, however, it is heavily T_2^* weighted, which limits the signal to noise ratio achievable [12]. Single Point Imaging (SPI) is a pure phase encode technique that can be implemented with very short dephasing times and is therefore well suited to imaging short T_2 and T_2^* materials. However, relatively long acquisition times are required, even with fast SPI techniques such as SPRITE [9]. Slice selection with pure phase encoding is also a challenge so it is commonly used for three dimensional rather than two dimensional acquisitions, further increasing the acquisition time. Other techniques commonly used for short T_2 and T_2^* materials are sweep imaging with Fourier transformation (SWIFT) [13] and zero echo time (ZTE) [14], however these are also not slice selective. UTE

---

potentially provides a method for rapidly imaging heterogeneous material with slice selection.

The acquisition time for UTE images may still be too long for studying evolving systems such as fluidized beds. Recently, CS has been introduced to reduce the acquisition time of MRI experiments by up to an order of magnitude [3,15,16]. CS works by exploiting the natural structure of MR images to reconstruct images accurately from partially sampled k-space data. CS has been applied to many systems [17–21] and pulse sequences but to the authors knowledge, has not yet been used with UTE.

One of the challenges associated with implementing UTE is ensuring that the gradient shape is generated accurately. It is well known that the gradient shape produced by the gradient amplifiers and coil does not match the input gradient perfectly. The error in gradient shape is typically corrected through the gradient pre-emphasis. However, the pre-emphasis may not produce the exact input gradient especially when short ramp times are used as in UTE. In most imaging sequences the remaining error is small enough that it does affect the final image. UTE is sensitive to the shape of the slice selection gradient, therefore it is desirable to ensure the gradient shape is accurate. A recently published technique by Goora et al. [22] introduces the idea of gradient pre-equalization as a technique to correct for the induced errors in gradient shape when using a short ramp. Their approach is applicable on almost any hardware platform and therefore is appealing for UTE imaging applications in material science and chemical engineering.

In this paper, common artifacts associated with the slice selection in UTE are illustrated using simulations of the Bloch equation. Experimental measurements are then used to demonstrate the implementation of accurate slice selection using UTE. In order to ensure accurate slice selection, the shape of the slice selection gradient was optimized by introducing the gradient pre-equalization of Goora et al. [22]. To reduce the acquisition time without introducing artifacts CS is used for image reconstruction. The UTE sequence is developed using a sample of doped water and the potential of UTE is demonstrated using samples of cork and rubber that have short T_2^* and T_2.

2. Background of UTE

UTE uses a soft excitation pulse, typically of a half Gaussian shape, to minimize the echo time (TE) [23]. Slice selection is achieved by applying a gradient at the same time as the soft pulse. When using a full Gaussian pulse, a second gradient is used to refocus the spins that have dephased during the second half of the radiofrequency (r.f.) pulse. This gradient must have the same area, but opposite sign, as that used during the second half of the r.f. pulse. Therefore, the refocusing gradient is typically of half the duration of the r.f. pulse. The duration of the refocusing gradient limits the minimum TE for slice selective excitations. The minimum TE for the sequence would occur if the acquisition were to begin immediately after the negative gradient lobe typically corresponding to around 0.5 ms or more. UTE overcomes this limitation by using the half shape which is formed by truncating the full shape at the zero phase point [24]. As the excitation ends at the zero phase point, the refocusing gradient is not needed and the acquisition can begin as soon as the r.f. pulse ends. However, as the excitation is truncated it gives a dispersion excitation, that is an excitation with both real and imaginary terms. To eliminate the imaginary component of the excitation the sequence needs to be executed twice. The two acquisitions are identical except that the slice select gradient has opposite sign. The sum of these two acquisitions produces an identical slice to that produced by a full Gaussian and refocusing gradient as the imaginary signals, i.e.

the dispersion peaks, cancel and the real signals, i.e. the absorption peaks, add [24].

A half Gaussian excitation requires the slice gradient to be switched off at the same time as the r.f. pulse ends. In practice it is impossible to switch off a gradient immediately owing to limitations in the slew rate that can be achieved by the gradient hardware. It is therefore necessary to switch the gradient off relatively slowly using a ramp. However, as the gradient strength decreases the instantaneous, apparent slice thickness of the r.f. pulse increases. Variable Rate Selective Excitation (VERSE) [25,26] is used to reshape the r.f. pulse to account for the time varying strength of the slice gradient. The VERSE pulse is designed such that the real-space bandwidth of the pulse remains constant as the gradient is decreased. A constant bandwidth is achieved by decreasing the power of the r.f. pulse, whilst increasing its duration and keeping the total applied power constant. This allows for the r.f. and gradient pulses to be switched off simultaneously.

In order to minimize T_2^* weighting, acquisition in a UTE sequence starts as soon as possible after the slice gradient switches off, typically about 10–50 μs is required to allow for ring down of the coil. As the acquisition starts immediately, a center out, non-Cartesian, sampling of k-space is required as there is no time for a phase encode gradient or de-phasing read gradient [24]. Typically k-space is sampled radially however, spiral sampling has also been used for samples with a somewhat longer signal lifetime [6]. A center out sampling pattern is desirable as it minimizes the echo time and ensures maximum signal sampled at the center of k-space. A drawback of non-Cartesian sampling is that it prevents the use of the fast Fourier transform (FFT), and therefore image reconstruction becomes prohibitively time consuming for many images. To overcome this limitation, "re-gridding" techniques have been developed to interpolate the measured signal onto a regular Cartesian grid which can then be transformed using the FFT [27]. It is important to choose the convolution function for this interpolation process accurately. Theoretically, a sinc function of infinite extent should be used, however, this is not practical. Common alternative convolution functions include truncated sinc interpolation, Kaiser–Bessel interpolation and min–max interpolation [28,29]. Such re-gridding techniques permit image reconstruction in almost the same time as with Cartesian sampling.

Non-Cartesian sampling, especially radial sampling, acquires data non-uniformly throughout k-space. In the case of radial sampling, many more points are acquired at the center of k-space (i.e. in the low spatial frequency region). If all data points are weighted equally, the Fourier transform would be biased to these low frequency data resulting in a low spatial resolution, or heavily blurred, image. Density compensation is used to overcome this limitation [30]. Density compensation considers the sampling density throughout k-space and uses a weighting function to correct for this. For radial sampling the weighting function will increase the contribution of the points around the edge of k-space prior to re-gridding and Fourier transformation.

Re-gridding with density compensation alone can produce blurring and artifacts in the reconstructed image, especially if the number of lines in the radial sampling pattern is small. An alternative approach is to iteratively reconstruct the image based on the a priori assumption that the unknown spin proton density image is sparse with respect to a specific representation. This assumption results in nonlinear optimization methods such as CS [3,16–19].

3. Methods

All experiments were performed using a Bruker, AV400 spectrometer, operating at a ^{1}H resonance frequency of 400.23 MHz. A three-axis, shielded gradient system with a maximum strength

of 146 G cm^{-1} was used for gradient encoding, and a 25 mm diameter birdcage r.f. coil was used for excitation and signal detection.

3.1. Numerical simulations

The Bloch equations were used to simulate artifacts that can arise during UTE slice selection. The Bloch equations describe the evolution over time of the magnetization in x, y, and z (M_x, M_y, and M_z) as a function of the strength of the homogeneous magnetic field (B_0), any applied gradients in the magnetic field (G), transverse relaxation (T_2), and longitudinal relaxation (T_1).

$$\frac{dM_x}{dt} = \gamma M_y(B_0 + G \cdot r) - \frac{M_x}{T_2} \tag{1}$$

$$\frac{dM_y}{dt} = -\gamma M_x(B_0 + G \cdot r) - \frac{M_y}{T_2} \tag{2}$$

$$\frac{dM_z}{dt} = -\frac{(M_z - M_0)}{T_1} \tag{3}$$

The Bloch equations were solved in Matlab using numerical integration [31]. A homogeneous sample of length 5 mm was used and resolved with a spatial resolution of 0.1 mm. The temporal resolution of the r.f. and gradient shape was 1 μs.

The Bloch equations were used to compare three different slice selection profiles for a 1024 μs full Gaussian pulse, a 512 μs half Gaussian pulse with positive and negative slice selection and a 537 μs VERSE pulse with positive and negative slice selection. The 537 μs VERSE pulse was then used for artifact simulation. The potential artifacts arising from errors in timing during UTE slice selection were simulated, with the gradient pulse switching off 10 μs before or after the VERSE r.f. pulse. The latter shows a similar artifact as would be obtained if VERSE were not used, as in that case the ramp down of the gradient will be longer than the ramp down of the r.f. pulse.

3.2. Experimental

The implemented pulse sequence for UTE is shown in Fig. 1. The sequence can be split into two almost identical parts, each consisting of an excitation pulse and slice select gradient, a set delay or TE, then the acquisition. The acquisition is displayed as a free induction decay (FID) during which gradients in both the x and y direction are ramped up to acquire radially sampled data as shown in Fig. 1b. The spokes are sampled from the center out which means that the maximum signal of the FID is sampled in the center of k-space. The only difference between the first and second half of the sequence is the sign of the slice select gradient. The acquired data from both the positive and negative slice select experiments are added prior to using a re-gridding approach to obtain the image. Here, the re-gridding algorithm of Fessler and Sutton is used [29].

The sensitivity of an MRI sequence to T_2 relaxation is characterized by the TE which is a measure of the T_2 or T_2^* weighting of a sequence and, in this study, refers to the time after excitation at which the center of k-space is acquired. If the signal lifetime is shorter than the TE, there will be little signal left during acquisition and hence the signal to noise ratio (SNR) of the image will be low and in the limit approximately zero. In a spin echo, TE is defined as twice the time between the 90° and 180° pulses, or the time from the zero phase point of the excitation to the peak of the spin echo; the gradient echo and spin echo coincide. The minimum TE for a spin echo is on the order of 1 ms. In a gradient echo sequence TE is defined as the time between the excitation and center of the gradient echo, and the minimum TE that is achievable is typically on the order of 0.5 ms. In UTE, the TE is defined as the time between the end of the r.f. pulse and the beginning of the data acquisition, a
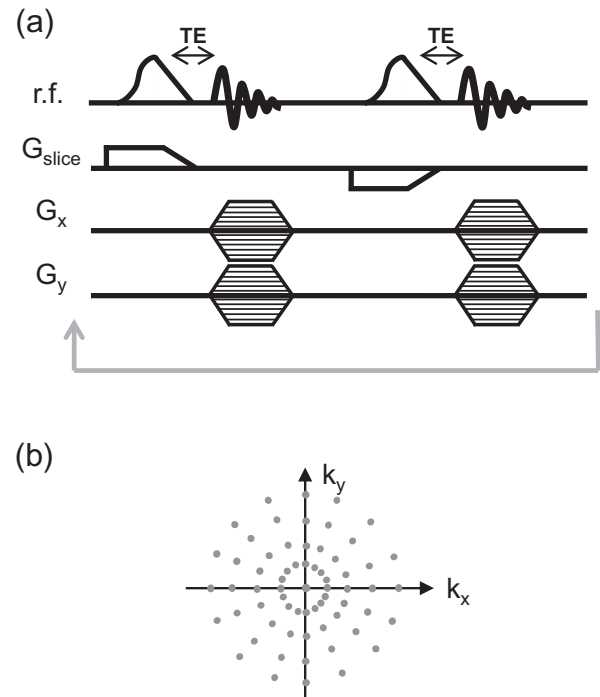

Fig. 1. (a) Two dimensional UTE imaging sequence. A ramped, half Gaussian, slice selective, soft pulse is used for excitation. Two excitations are used for each line acquired in k-space to produce a Gaussian shaped slice selection. (b) k-Space is mapped radially by varying the strength of the x and y gradients.

center-out trajectory is used hence the TE can be short. Typically a TE of 100–250 μs is used, however times as short as 8 μs have been reported [6].

The implementation of the sequence can be separated into two key areas: (i) the implementation of slice selection and (ii) the image reconstruction. Each of these aspects of the UTE sequence will be affected by the particular hardware used. In the following we discuss both aspects of UTE and present a simple technique to visualize the slice excitation profile.

3.2.1. Implementation of slice selection

The r.f. and gradient shape must be well matched to ensure accurate slice selection. Here, the slice select gradient is ramped down from constant strength to zero over a few microseconds. The r.f. pulse for UTE excitation was reshaped to match the gradient using VERSE [26]. To apply VERSE, the center point of the gradient ramp is placed at the original end point of the half Gaussian r.f. pulse. The VERSE principle is then used to reshape the r.f. pulse to match the ramped switch off of the slice gradient. The r.f. pulse is scaled such that the area of the new pulse shape is equivalent to that of the original half Gaussian r.f. pulse. The use of VERSE compensates for the limited slew rate achievable by the gradient amplifiers and helps to ensure accurate slice selection. For the experiments shown here, the gradient pulse was defined with a 50 μs linear ramp from the constant value to zero and the r.f. ramp down time was therefore set to match this.

The oscilloscope can be used to measure the output gradient shape from the amplifiers; however, there is still some variation between the amplifiers and the gradient input to the sample. It is therefore desirable to measure the applied gradient directly. Here, the applied gradient is measured using the technique of Duyn et al. [32]. The sequence measures the phase change across a thin slice in a homogeneous sample. This phase change corresponds to a direct measurement of position in k-space. The derivative of the

measured phase change provides the strength of the gradient that is produced by the gradient coil as a function of time.

Using measurements of the gradient, the shape of the gradient is corrected using a method known as gradient pre-equalization [22]. The method is outlined in Fig. 2. Initially, the input gradient is defined as a step function, $u(t)$, that switches instantaneously from zero to a constant value. The resulting output, $y(t)$, is measured using the gradient measurement technique of Duyn et al. [32]. The measured gradient shape is then used to approximate the impulse response, $h(t)$, of the gradient amplifier and coils. The impulse response is a feature of the system being used and is approximated as the derivative of the measured output gradient in response to an input step function:

$$\frac{d}{dt}y(t) = h(t). \tag{4}$$

The impulse response is then used to estimate the input function to the gradient amplifier, $x_p(t)$, that is required to achieve a desired output gradient shape, $y_d(t)$.

$$x_p(t) = F^{-1}\left\{\frac{F[y_d(t)]}{F[h(t)]}\right\}. \tag{5}$$

Eq. (5) describes a deconvolution of the impulse response from the desired shape. Deconvolution is prone to amplifying noise as it involves division in the frequency domain. To overcome this, Goora et al. [22] model their measured gradient using a polynomial. Here, we use a Gaussian filter, with a standard deviation of 200,000 Hz, in the Fourier domain to suppress the noise. The resulting shape is then applied to the MRI system and the output gradient shape is measured using the method of Duyn et al. [32].

An oscilloscope is used to measure the approximate timing of the r.f. and gradient pulses. The time at which the r.f. pulse is applied is adjusted until the two pulses end at the same time. This timing is later optimized experimentally as there is a slight delay of approximately 20 μs between the input from the gradient amplifier and the actual applied gradient. The optimization is performed using the slice measurement technique that will be described in Section 3.2.3.

3.2.2. Image reconstruction

The k-space data for UTE is acquired on a non-Cartesian grid. The NUFFT algorithm of Fessler and Sutton [29] is used to perform the re-gridding and subsequent fast Fourier-transformation of the k-space data points. The k-space trajectory is measured using the
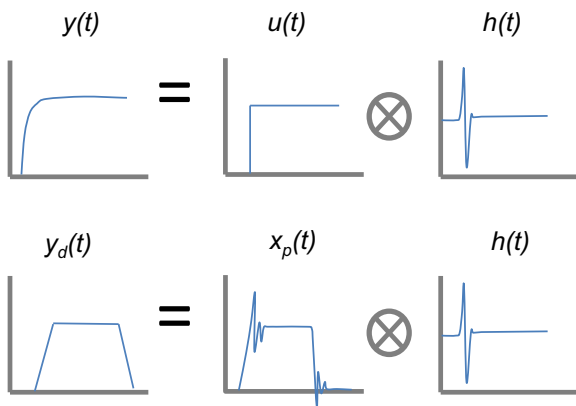
technique of Duyn et al. [32] as accurate image reconstruction requires precise knowledge of the trajectory. The images are reconstructed using the total variation based regularization method as described in Benning et al. [33]. A brief description of the approach used here is

$$u_{\alpha,\beta} \in \arg\min_u\left\{\frac{1}{2}||Fu - f||_2^2 + \alpha||\nabla u||_{2,1} + \beta||u||_1\right\} \tag{6}$$

which is a Tikhonov-type reconstruction with total variation prior and, in the context of under sampled MRI, is often referred to as CS [3]. Here u denotes the spin density image, F the non-uniform fast Fourier transform (NUFFT) operator, ∇ a forward finite difference discretization of the gradient operator, $||u||_1$ the one-norm, $||\nabla u||_{2,1}$ the one-norm applied to $\sqrt{(\nabla_x u)^2 + (\nabla_y u)^2}$, α the regularization parameter for the gradient term, β the regularization parameter for the image, f the measured k-space data and $u_{\alpha,\beta}$ the image to be recovered. Lustig et al. [17] used a similar method (with $||\nabla u||_{1,1}$ instead of $||\nabla u||_{2,1}$) as an optimization method as it had been shown to successfully overcome the blurring and ringing artifacts present in the zero-filled reconstruction. The regularization parameters, α and β, are chosen heuristically. For robust methods used to select regularization parameters see Benning et al. [33].

3.2.3. Measurement of slice

The slice selection profile was measured using the one dimensional imaging sequence shown in Fig. 3. The sequence uses a frequency encoded acquisition applied in the same direction as the slice selection. Two homospoil pulses, one on either side of the 180° hard pulse, and a four step phase cycle are used to ensure that only signal relating to the spin echo is detected. As in the 2D sequence, there are two acquisitions, which will be added together to measure the slice that has been selected. Both acquisitions are Fourier transformed to show the real signal as an absorption peak and the imaginary signal as a dispersion peak. These can be added together to achieve a purely real Gaussian excitation. The slice measurement sequence is used to ensure accurate timing of the r.f. excitation and slice select gradient, such that these end simultaneously. A pure phase encode method was also tested for imaging the slice selection. The results were equivalent.

The slice bandwidth was measured from the full width at half of the maximum (FWHM) of the real excitation profile. The absolute value could also be used for the optimized acquisition as the imaginary signal is zero. The measured slice bandwidth was used to calculate the slice thickness in subsequent UTE imaging experiments.

3.2.4. Samples

Four samples are used in this study. A homogeneous sample of doped water is used for all gradient measurements and for 1D slice selection imaging. The water is doped with 0.23 mM gadolinium chloride to give a T_1 of 120 ms and a T_2 of 105 ms. To test the UTE imaging sequence, two samples are used with different T_2 and T_2^* relaxation times. The second sample was comprised of 5 mm glass beads randomly packed into a 20 mm inner diameter glass tube. The glass beads were surrounded by water doped with 0.23 mM gadolinium chloride. The sample has a T_1 of 690 ms, T_2 of 540 ms, and a T_2^* of 2 ms. The third sample is composed of two rectangular pieces of cork with a T_1 of 420 ms and a T_2^* of 0.12 ms. The T_2 for the cork was too short to measure with the available hardware however is assumed to be less than 0.5 ms and likely on the order of the T_2^*. The fourth sample is comprised of 10 mm glass beads surrounded by rubber particles (a cured blend of thermoset rubber, SoftPoint Industries Inc.). The T_2^* of the rubber is approximately 75 μs and, again, it is not possible to measure T_2 with the available hardware. The bead pack is used to quantify the accuracy

Fig. 2. The principle of the method used to calculate the impulse response function of the gradient on a specific instrument is shown. The impulse response of the system is calculated from the derivative of the measured step. The impulse response function can then be used to determine the necessary input shape that will produce the desired gradient shape.
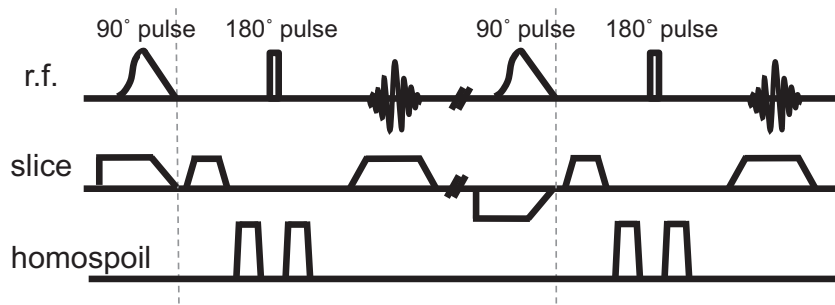
Fig. 3. The one dimensional pulse sequence used to measure the slice selected in a UTE sequence is shown. The excitation is the same as is seen in the 2D sequence however, a 180° pulse is added to form a spin echo. The two acquisitions will be added to show the shape of the slice selected.

of slice selection during imaging by providing a system on which both spin echo and UTE can be used. Cork and this rubber both have a short T_2 and T_2^* making them impossible to image with a spin echo technique, and good candidates for UTE imaging.

3.2.5. Experimental details

The development of the r.f. excitation pulse for the UTE imaging sequence started with a 1024 μs Gaussian pulse, 1500 Hz FWHM. The re-shaped VERSE excitation pulse was 537 μs in length. A slice selection gradient of 5.1 G cm^{-1} was used to give a 1 mm thick slice. Both r.f. and gradient pulses were switched off using a 50 μs ramp. A ring down delay of 10 μs was set before the acquisition started. The acquisition gradient strength was increased over 50 μs prior to reaching a maximum value of 10.6 G cm^{-1}. Each of 64 radial spokes was acquired with a sweep width (SW) of 10^6 and 400 complex points. The images are reconstructed on a 128×128 pixel grid corresponding to a resolution of 0.2 mm × 0.2 mm × 1 mm with a 25 mm FOV. The sequence is run with a two-step phase cycle to eliminate the DC offset and the total acquisition time for the image was 2 min.

The second UTE sequence is run using the same parameters, however, only one average with 32 spokes of data is acquired and a 10° tip angle is used to further reduce the acquisition time. The total acquisition time for this sequence was 500 ms.

Slice selection was validated using a uniform sample of doped water and the pulse sequence shown in Fig. 3. The slice select gradient was set to 5.1 G cm^{-1} and the acquisition gradient was set to 11.7 G cm^{-1}. The homospoil pulses were set to 22.0 G cm^{-1} and had a duration of 1 ms with a 5 ms delay before and after the 180° hard pulse. The SW was set to 10^6 and 512 complex points were collected.

As a comparison for the UTE image, a spin echo image was run for each sample. The spin echo used a TE of 3 ms with a resolution of 0.2 mm × 0.2 mm × 1 mm. A 512 μs Gaussian pulse was used for slice selection and the SW was set to 10^5. The total acquisition time for the image was 4 min.

4. Results

In the following, UTE is first simulated using the Bloch equations to demonstrate the concept and illustrate the artifacts that commonly arise during slice selection. The gradient optimization and slice selection are then explored. The accuracy of UTE image reconstruction is demonstrated using a challenging sample with a complex three dimensional structure. The benefits of UTE are then shown by imaging two samples, one of cork and one of rubber. Finally, the potential for dynamic imaging is explored using CS.
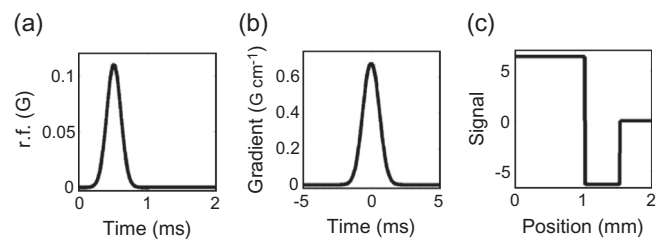

Fig. 4. Simulation of a conventional slice excitation. The Gaussian r.f. excitation is shown in (a). The timing of the pulse is matched with the gradient (b). The gradient is constant during the pulse and has a negative, refocusing, lobe after the pulse equaling half of the area of the gradient during the pulse. (c) Shows a simulation of the slice selected using the r.f. and gradient pulses from (a) and (b).

4.1. Slice selection: simulation

Fig. 4 shows a simulation of the Bloch equations for a typical Gaussian slice selection. A Gaussian r.f. excitation pulse is used with a gradient on for the duration of the r.f. pulse. The gradient is then applied in a negative direction for half of the time of the r.f. pulse with the same magnitude as during the r.f. pulse. The negative gradient acts to rephase the spins that have been dephased during the second half of the r.f. pulse. The slice selected by this sequence is a Gaussian shape as expected. The slice selection for UTE attempts to emulate the shape of the slice selected using this traditional method of slice selection, but using a half Gaussian pulse to reduce TE.

Fig. 5 shows the equivalent slice selection performed using UTE. UTE uses a half Gaussian pulse for soft pulse excitation, which eliminates the need for a negative refocusing gradient. However, the half-Gaussian pulse results in the formation of a complex dispersion mode excitation profile. To select a Gaussian slice, the
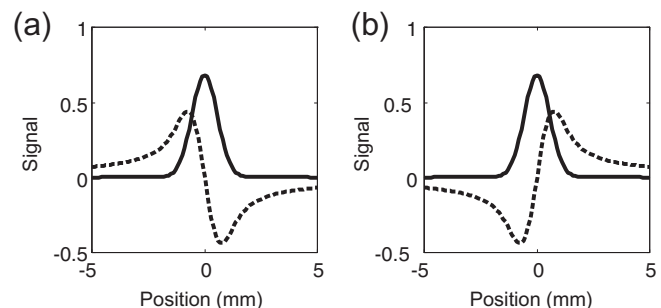

Fig. 5. Simulations of the slice excited using (a) a positive slice selection gradient and (b) a negative slice selection gradient. The imaginary signals, denoted by the dotted line, are exactly opposite. The real signals, denoted by the solid line are identical. Thus, the sum of (a) and (b) would produce a purely real slice selection.
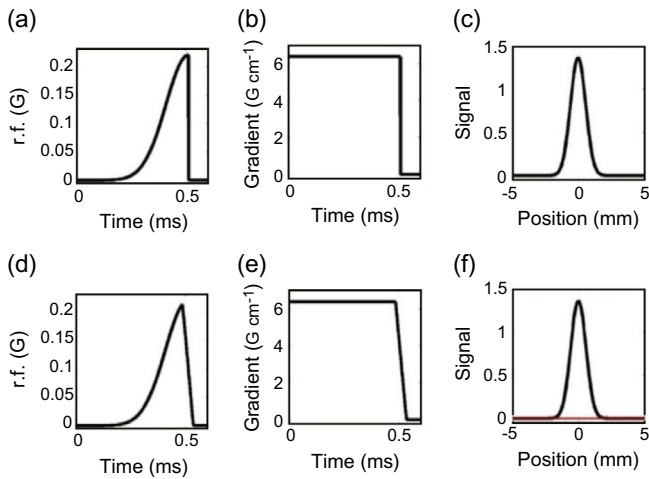
Fig. 6. Simulations of conventional and VERSE UTE slice selection. The r.f. excitation shape is shown in (a and d) with the corresponding gradient shown in (b and e). The slice selected from these is shown in (c and f). Half Gaussian (a–c) and VERSE (d–f) excitation pulses are shown to excite identical slices. The red line in (f) shows the difference between the slice selection in (c) and (f). (For interpretation of the references to colour in this figure legend, the reader is referred to the web version of this article.)
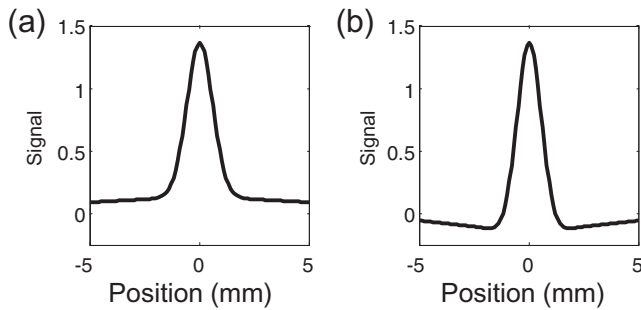

Fig. 7. Figures (a) and (b) show common slice artifacts obtained using the UTE, VERSE excitation. The results are obtained from simulations of the Bloch equations. If the gradient ends 10 μs before the r.f. pulse as shown in (a), the r.f. pulse excites signal outside the desired slice. This can be seen as the Gaussian slice does not decay to zero outside the desired shape. If the gradient ends 10 μs after the r.f. pulse, as shown in (b), the r.f. pulse produces lobes of signal outside the desired slice with incorrect phase, in this case a negative phase is seen.
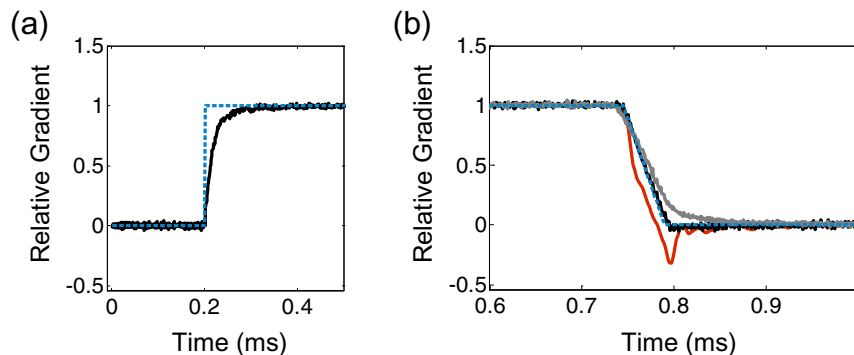
acquisition must be run twice, once with a positive slice select gradient and once with a negative slice select gradient. The imaginary slice profile for these two acquisitions will be in anti-phase, as shown in Fig. 5. Therefore, the addition of the two acquisitions results in a purely real excitation profile, as desired.

Fig. 6 shows simulations of the ideal and VERSE excitation. In each case, the slice selection was run twice, once with a positive gradient and once with a negative gradient, then added together; only the positive gradient is shown in (b) and (e). Fig. 6a shows exactly half of a Gaussian shaped r.f. excitation, and Fig. 6b shows the corresponding slice gradient. The slice selected, Fig. 6c, is identical to that using a full Gaussian pulse with a negative refocusing gradient lobe. Experimentally, it is impossible to turn off the gradient pulse instantaneously. Therefore, VERSE is used to decrease the r.f. power with the gradient such that the real space bandwidth of the soft pulse is constant. Fig. 6(d) and (e) show the r.f. and gradient pulses after VERSE correction. The resulting slice excitation is shown in Fig. 6f and it is clear that the slice selected is identical to that selected by both the half Gaussian and the full Gaussian pulses.

The simulations shown in Figs. 4–6 demonstrate that slice selection using a half Gaussian pulse in combination with VERSE can be used to eliminate the time required for the negative refocusing gradient, as is well established [23]. These simulations can also be used to explore what happens when the timing in the pulse sequence is not accurate.

Fig. 7 illustrates two common artifacts that can arise with UTE even when using the VERSE pulse. In Fig. 7a, the gradient switches off 10 μs before the r.f. pulse. The majority of the pulse takes place while the gradient is on, hence the correct slice is initially excited. However, as the r.f. pulse continues after the gradient is turned off, the last part of the r.f. pulse excites the whole sample rather than only the desired slice. Therefore, the excited slice is seen to have signal from both the correctly excited slice and the sample outside the intended slice. If this experiment was used for slice excitation, the slice would be poorly defined with a large portion of signal arising from outside the desired slice.

Another common artifact occurs when the gradient switches off after the r.f. pulse. Spins are dephased during the time that the gradient is on without the r.f. pulse which causes a first order phase change across the sample that is different for the positive and negative slice selection experiments. Fig. 7b demonstrates the slice selection artifact that arises when the gradient switches off 10 μs after the r.f. pulse. The signal has a negative lobe on either side of the desired slice. Thus, this error in timing also results in a poorly defined slice. In practice, it is the integral of the complex slice profile that is detected in each pixel. Therefore, if the gradient ends after the r.f. pulse the image will be difficult to interpret as
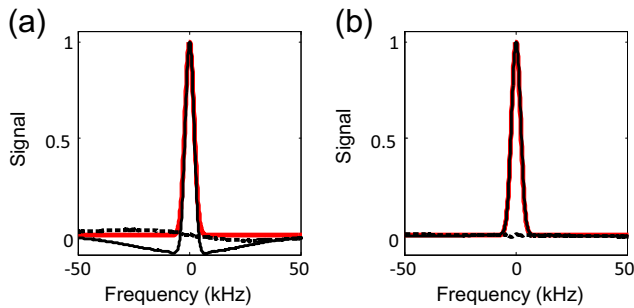

Fig. 8. The experimental step response function of the gradient is shown in (a). The ideal gradient is given by the dashed blue line while the measured step response is given by the solid black line. The gradient shape used for UTE is shown in (b). As in (a), the dashed blue line indicates the ideal shape. The solid black line indicates the measured shape with gradient pre-equalization. It is difficult to differentiate between the two in this figure. The red line denotes the input to the gradient amplifier required to produce the measured gradient, black line, in (b). The grey line shows the measured gradient obtained when the desired shape is used as the input to the gradient. (For interpretation of the references to colour in this figure legend, the reader is referred to the web version of this article.)

Fig. 9. Experimentally measured slice selection (a) without using gradient pre-equalization and (b) with gradient pre-equalization. Real, solid black line, and imaginary, dashed black line, signal for UTE slice selection is shown after addition of the signal from acquisition with positive and negative gradients applied during the soft pulse. The experimental signal is overlaid on an ideal Gaussian shape, solid red line. (For interpretation of the references to colour in this figure legend, the reader is referred to the web version of this article.)

the negatively excited signal above and below the desired slice will cancel out the positively excited signal from within the slice. A similar artifact would be observed if the r.f. pulse were not corrected using VERSE.

4.2. Slice selection: experimental

Fig. 8a shows the measured step response of the gradient. The corners of a gradient shape are typically rounded, as can be seen in the step function measured in Fig. 8a. This causes difficulty in matching the relative timing between the gradient and r.f. pulses as the tail on the gradient ramp down can add phasing effects to the selected slice. Fig. 8b shows the desired gradient shape, the output measured when using the desired gradient shape, the input function estimated using pre-equalization to achieve the desired shape, and the output measured when using the pre-equalized input gradient shape. The output in Fig. 8b is shown to closely match the desired gradient shape, in fact, it is difficult to resolve the difference between the gradient output and desired shape. Thus, the gradient pre-equalization produces a higher quality output with greater definition at the corners of the desired shape in comparison with the rounded corners of the measured gradient when using the desired shape as the input. The corrected gradient shape will help ensure accurate slice selection in UTE imaging.

To test the relative timing between the r.f. and gradient pulses, a series of slice profiles were acquired by shifting the r.f. pulse, relative to the gradient, in 1 µs intervals. The slice profiles shown in Fig. 9 were acquired using the optimized relative timing. The figure shows an ideal Gaussian shape along with both the real and imaginary signals for the selected slice. This profile was obtained by adding acquisitions with both positive and negative gradients applied during slice selection. The profile in Fig. 9a is using a ramped gradient without pre-equalization. It can be seen that the "tail" on the gradient has a significant effect on the profile of the selected slice and the artifact shown is similar to the simulation in Fig. 7b. Fig. 9b shows the slice selection when using gradient pre-equalization. The combined real signal is a Gaussian shaped peak and the imaginary signal is effectively zero, in good agreement with the Bloch equation simulations shown in Fig. 6. The experimentally measured slice profile closely emulates that simulated using the Bloch equations.

4.3. Imaging

UTE images using the optimized protocol from Section 3.2 were acquired of a bead pack with doped water. This sample can be accurately imaged using both spin echo and UTE pulse sequences as the T_2 is within the limits of spin echo imaging. Images of the bead pack are used to confirm the accuracy of the UTE imaging
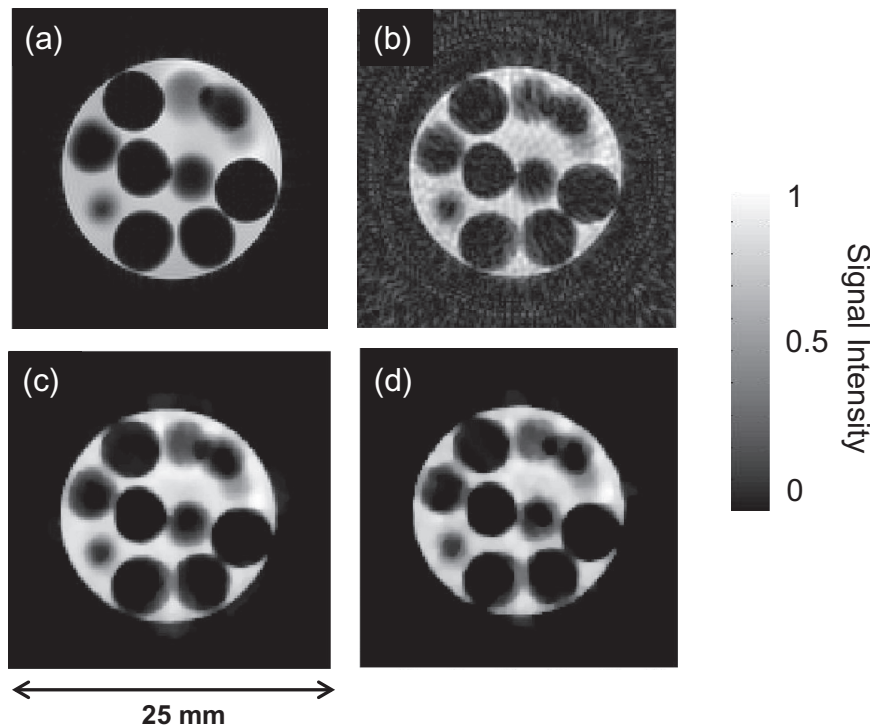

Fig. 10. (a) Spin echo and (b–d) UTE images of a bead pack filled with doped water. UTE images are reconstructed using (b) a NUFFT with density compensation algorithm, (c) CS with $\alpha = 0.001$, $\beta = 0.01$ and (d) CS with $\alpha = 0$, $\beta = 0.01$. The acquisition time for the spin echo image was approximately 4 min with a TE of 3 ms. The UTE reconstruction in (b and c) was done using 64 center-out, radial spokes corresponding to an image time of approximately 2 min with a TE of 10 µs. The reconstruction in (d) used only 32 center-out radial spokes reducing the acquisition time by half, to approximately 1 min with the TE remaining at 10 µs. All images are shown with a field of view of 25 mm × 25 mm and a spatial resolution of 0.2 mm × 0.2 mm with a 1 mm slice thickness.

sequence. The spin echo image, in Fig. 10a, shows clear edges around five beads that are directly in plane and has blurred edges around the beads that are partially in plane. The UTE image in Fig. 10b was reconstructed using re-gridding and density compensation. The image in Fig. 10c was reconstructed using CS. The structure of the bed is recovered clearly in all three images, though the image in Fig. 10b is much "noisier" than that in Fig. 10a or c. The "noise" in Fig. 10b is primarily an artifact arising from the partial sampling of k-space used here. This artifact is eliminated by reconstruction with CS, as in Fig. 10c. There is some evidence of blurring in the UTE images shown in Fig. 10, especially where the beads touch the walls. This is likely due to slight errors in the k-space trajectory measurement [34]. However, overall the resolution of all three images is essentially equivalent, demonstrating the potential for UTE to obtain high-resolution images of complex samples.

The UTE images shown in Fig. 10b and c were acquired using 64 center-out, radial spokes. Thus, these images were already obtained from only one quarter of the radial spokes required for a complete sampling of k-space at a resolution of 128 × 128 pixels. To further demonstrate the strength of the CS algorithm when reconstructing under sampled images, an image of the bead pack is shown in Fig. 10d obtained with only 32 center-out, radial spokes. The acquisition time of this image is 1 min, half of that used for the images in Fig. 10b and c and an eighth of the time that would be required for a fully sampled center-out radial image. The intensity of the reconstructed image exhibits slightly more of the classic "stair-case" artifact [35], however, the structure of the bead pack is recovered accurately, with a clear demarcation between the solid beads (no signal) and the water. Indeed the image is very similar in quality to the UTE image acquired using all 64 radial spokes shown in Fig. 10c.

To demonstrate the strength of the UTE sequence for imaging short T_2 material, we compare UTE and spin echo images of cork. A schematic of the sample is shown in Fig. 11a. The T_2 of cork is much less than the minimum TE of the spin echo sequence, therefore there is no signal from the sample in the spin echo image shown in Fig. 11b. In contrast, the UTE image, in Fig. 11c, clearly shows the existence of a sample of cork. According to theory, the optimal bandwidth for the acquisition is defined by:

$$\frac{1}{T} = \frac{N\pi}{T_2^*} \tag{7}$$

where T is the dwell time and N is the number of points in one image dimension [12]. Considering the sample of cork, the optimal dwell time for a 128 × 128 image would be 0.05 μs. This is not
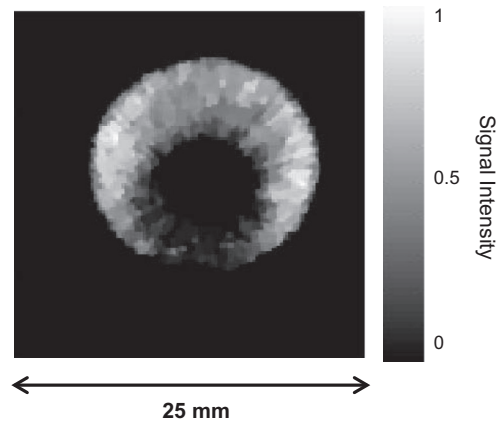

Fig. 12. UTE images of rubber particles around a glass bead acquired with 32 center-out radial spokes. The image is reconstructed using CS with $\alpha = 0.00016$, $\beta = 0.06$. The image is 25 mm × 25 mm with a spatial resolution of 0.2 mm × 0.2 mm with a 1 mm slice thickness. The acquisition time was approximately 500 ms with a TE of 10 μs.

achievable with the present hardware, thus the image resolution is linewidth limited when using the minimum achievable dwell time of 1 μs per complex point. In a linewidth limited system with exponential decay, the resolution is defined by:

$$\Delta x = \left(\frac{1}{\pi T_2^*}\right)\left(\frac{2\pi}{\gamma G}\right) \tag{8}$$

where γ is the gyromagnetic ratio of the nucleus and G is the acquisition gradient strength [12]. However, as the gradient must ramp up to reach the constant value in UTE, the true resolution will be less than this. The ramp is on for 50 μs, with a 10 μs initial delay. The ramp up can be used to estimate the actual signal decay at each point in k-space. The resulting point spread function is no longer a Lorentzian shape, but the resolution limit can be estimated to be approximately 400 μm from the FWHM, or 2 pixels at the image resolution considered here. Two rectangular pieces of cork are used to show the obtainable resolution in the image in Fig. 11b. It is possible to resolve the gap between the pieces, though this was too small to measure physically.

To further demonstrate the advantage of UTE, Fig. 12 shows an image of 10 mm glass beads surrounded by rubber particles. The T_2^* for the rubber is 75 μs making it difficult to image with conventional techniques, however, the signal from the rubber is well
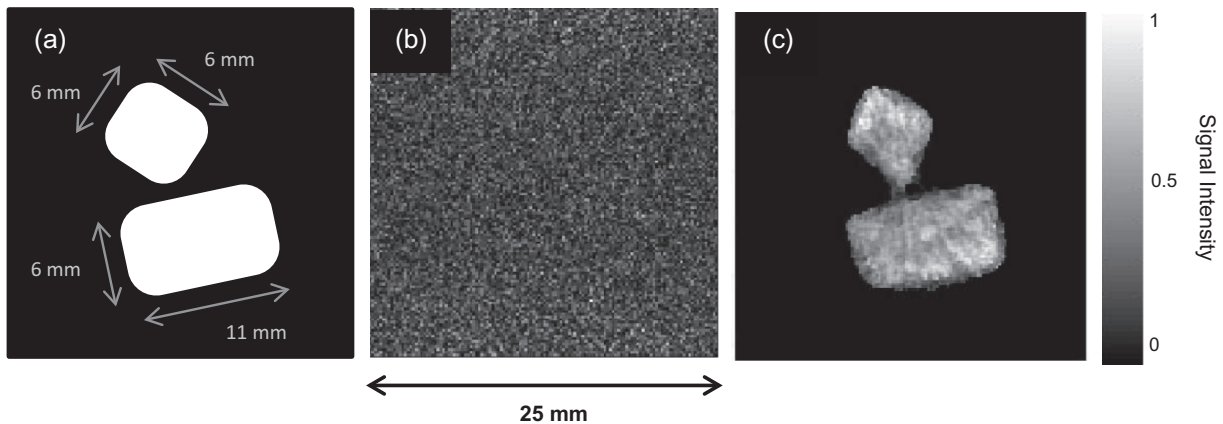

Fig. 11. (a) A schematic of the cork sample with dimensions is shown for comparison with (b) the Spin echo image and (c) the UTE image of cork. The UTE image is reconstructed using CS with $\alpha = 0.0025$ and $\beta = 1.8$. The TE in the spin echo is too long to acquire any signal whereas UTE can acquire data over the short signal lifetime of cork. Both images are shown with a field of view of 25 mm × 25 mm with a spatial resolution of 0.2 mm × 0.2 mm with a 1 mm slice thickness. The acquisition time for the spin echo was approximately 4 min with a TE of 3 ms and for the UTE was 2 min with a TE of 10 μs.

resolved. The boundary of the glass bead shown in Fig. 12 is jagged in appearance. The image was acquired using 32 center-out radial spokes and is therefore significantly under sampled in the azimuthal direction. Such under sampling could give rise to a jagged artifact but should be removed by the CS reconstruction. A more significant effect arises from the dimensions of the particles and the resolution of the image. The diameter of the rubber particles is 0.2–0.5 mm and close to the resolution of the image, 0.2 mm. Jagged or noise-like structure, as seen in Fig. 12, has frequently been seen in high resolution imaging of poppy seeds [36] where the diameter of the seeds is similar to the resolution of the image. The acquisition time of the image in Fig. 12 was 500 ms. Thus, these results demonstrate that UTE can provide high spatial and temporal resolution measurements on short T_2 and T_2^* samples.

5. Conclusion

UTE has been shown as an efficient method of imaging short T_2 and T_2^* systems. To accurately implement UTE it is necessary to have a thorough characterization of the gradients and r.f. amplifiers to be used. It is important to measure the shape of the r.f. and gradient pulses to determine whether these are balanced and timed correctly, especially when imaging short T_2^* materials. A gradient pre-equalization strategy was used to improve the fidelity of the slice gradient shape and hence the slice excitation profile. The gradient pre-equalization method should be applicable on almost any hardware system, including those commonly used in materials science and chemical engineering. The UTE sequence was validated using a sample that could also be imaged with a spin echo technique. The use of CS for image reconstruction significantly reduces the artifacts arising from under sampling and permits accurate image reconstruction from a reduced number of spokes, thus reducing the acquisition time. UTE was demonstrated on two simple test samples. In the future, the approach outlined here will enable UTE to be implemented on a variety of hardware systems and applications and hence will open new opportunities in engineering and material science.

Acknowledgments

References

[1] J.M. Pauly, S.M. Conolly, D.G. Nishimura, A. Macovski, Slice-selective excitation for very short T2 species, in: Proc. 8th Annu. Meet. SMRM, Amsterdam, 1989, p. 28.

[2] P.M. Margosian, T. Takahashi, M. Takizawa, Practical implementation of UTE imaging, Encycl. Magn. Reson. 1 (2012) 297–310, http://dx.doi.org/10.1002/9780470034590.emrstm1247.

[3] M. Lustig, D.L. Donoho, J.M. Santos, J.M. Pauly, Compressed sensing MRI, IEEE Signal Process. Mag. 25 (2) (2008) 72–82.

[4] K.R. O'Brien, S.G. Myerson, B.R. Cowan, A.A. Young, M.D. Robson, Phase contrast ultrashort TE: a more reliable technique for measurement of high-velocity turbulent stenotic jets, Magn. Reson. Med. 62 (2009) 626–636, http://dx.doi.org/10.1002/mrm.22051.

[5] H.T.C. Nielsen, G.E. Gold, E.W. Olcott, J.M. Pauly, D.G. Nishimura, Ultra-short echo-time 2D time-of-flight MR angiography using a half-pulse excitation, Magn. Reson. Med. 41 (1999) 591–599, http://dx.doi.org/10.1002/(SICI)1522-2594(199903)41:3<591::AID-MRM23>3.0.CO;2-R.

[6] J. Du, M. Bydder, A.M. Takahashi, C.B. Chung, Two-dimensional ultrashort echo time imaging using a spiral trajectory, Magn. Reson. Imaging 26 (2008) 304–312, http://dx.doi.org/10.1016/j.mri.2007.08.005.

[7] J. Du, M. Carl, M. Bydder, A. Takahashi, C.B. Chung, G.M. Bydder, Qualitative and quantitative ultrashort echo time (UTE) imaging of cortical bone, J. Magn. Reson. 207 (2010) 304–311, http://dx.doi.org/10.1016/j.jmr.2010.09.013.

[8] M.D. Robson, G.M. Bydder, Clinical ultrashort echo time imaging of bone and other connective tissues, NMR Biomed. 19 (2006) 765–780, http://dx.doi.org/10.1002/nbm.

[9] B. Blümich, NMR Imaging of Materials, Oxford University Press, New York, 2000.

[10] C.R. Müller, J.F. Davidson, J.S. Dennis, P.S. Fennell, L.F. Gladden, A.N. Hayhurst, et al., Real-time measurement of bubbling phenomena in a three-dimensional gas-fluidized bed using ultrafast magnetic resonance imaging, Phys. Rev. Lett. 96 (2006) 154504(4), http://dx.doi.org/10.1103/PhysRevLett.96.154504.

[11] C.R. Müller, D.J. Holland, A.J. Sederman, M.D. Mantle, L.F. Gladden, J.F. Davidson, Magnetic resonance imaging of fluidized beds, Powder Technol. 183 (2008) 53–62, http://dx.doi.org/10.1016/j.powtec.2007.11.029.

[12] P.T. Callaghan, Principles of Nuclear Magnetic Resonance Microscopy, Oxford science publications, New York, 1993.

[13] D. Idiyatullin, C. Corum, J.-Y. Park, M. Garwood, Fast and quiet MRI using a swept radiofrequency, J. Magn. Reson. 181 (2006) 342–349, http://dx.doi.org/10.1016/j.jmr.2006.05.014.

[14] M. Weiger, K.P. Pruessmann, MRI with zero echo time, Encycl. Magn. Reson. (2012).

[15] E.J. Candès, J. Romberg, T. Tao, Robust uncertainty principles: exact signal frequency information, IEEE Trans. Inf. Theory 52 (2006) 489–509, http://dx.doi.org/10.1109/TIT.2005.862083.

[16] D.L. Donoho, Compressed sensing, IEEE Trans. Inf. Theory 52 (2006) 1289–1306, http://dx.doi.org/10.1109/TIT.2006.871582.

[17] M. Lustig, D.L. Donoho, J.M. Pauly, Sparse MRI: the application of compressed sensing for rapid MR imaging, Magn. Reson. Med. 58 (2007) 1182–1195, http://dx.doi.org/10.1002/mrm.21391.

[18] D.J. Holland, D.M. Malioutov, A. Blake, A.J. Sederman, L.F. Gladden, Reducing data acquisition times in phase-encoded velocity imaging using compressed sensing, J. Magn. Reson. 203 (2010) 236–246, http://dx.doi.org/10.1016/j.jmr.2010.01.001.

[19] U. Gamper, P. Boesiger, S. Kozerke, Compressed sensing in dynamic MRI, Magn. Reson. Med. 59 (2008) 365–373, http://dx.doi.org/10.1002/mrm.21477.

[20] P. Parasoglou, D. Malioutov, A.J. Sederman, J. Rasburn, H. Powell, L.F. Gladden, A. Black, M.L. Johns, et al., J. Magn. Reson. 201 (2009) 72–80, http://dx.doi.org/10.1016/j.jmr.2009.08.003.

[21] A.B. Tayler, D.J. Holland, A.J. Sederman, L.F. Gladden, Exploring the origins of turbulence in multiphase flow using compressed sensing MRI, Phys. Rev. Lett. 108 (2012) 264505, http://dx.doi.org/10.1103/PhysRevLett. 108.264505.

[22] F.G. Goora, B.G. Colpitts, B.J. Balcom, Arbitrary magnetic field gradient waveform correction using an impulse response based pre-equalization technique, J. Magn. Reson. 238 (2014) 70–76, http://dx.doi.org/10.1016/j.jmr.2013.11.003.

[23] J.M. Pauly, Selective excitation for ultrashort echo time imaging, Encycl. Magn. Reson. 1 (2012) 381–388, http://dx.doi.org/10.1002/9780470034590.emrstm1271.

[24] M.D. Robson, P.D. Gatehouse, M. Bydder, G.M. Bydder, Magnetic resonance: an introduction to ultrashort TE (UTE) imaging, J. Comput. Assist. Tomogr. 27 (2003) 825–846.

[25] S. Conolly, D. Nishimura, A. Macovski, G. Glover, Variable-rate selective excitation, J. Magn. Reson. 78 (1988) 440–458, http://dx.doi.org/10.1016/0022-2364(88)90131-X.

[26] B.A. Hargreaves, C.H. Cunningham, D.G. Nishimura, S.M. Conolly, Variable-rate selective excitation for rapid MRI sequences, Magn. Reson. Med. 52 (2004) 590–597, http://dx.doi.org/10.1002/mrm.20168.

[27] M.E. Haacke, R.W. Brown, M.R. Thompson, R. Venkatesan, Magnetic Resonance Imaging: Physical Principles and Sequence Design, John Wiley and Sons, 1999.

[28] J.I. Jackson, C.H. Meyer, D.G. Nishimura, A. Macovski, Selection of a convolution function for Fourier inversion using gridding, IEEE Trans. Med. Imaging 10 (1991) 473–478, http://dx.doi.org/10.1109/42.97598.

[29] J.A. Fessler, B.P. Sutton, Nonuniform fast Fourier transforms using min-max interpolation, IEEE Trans. Signal Process. 51 (2003) 560–574, http://dx.doi.org/10.1109/TSP.2002.807005.

[30] R.D. Hoge, R.K. Kwan, G.B. Pike, Density compensation functions for spiral MRI, Magn. Reson. Med. 38 (1997) 117–128, http://dx.doi.org/10.1002/mrm.1910380117.

[31] B.A. Hargreaves, Bloch Equation Simulation (2002). http://mrsrl.stanford.edu/~brian/bloch/.

[32] J.H. Duyn, Y. Yang, J.A. Frank, J.W. van der Veen, Simple correction method for k-space trajectory deviations in MRI, J. Magn. Reson. 132 (1998) 150–153, http://dx.doi.org/10.1006/jmre.1998.1396.

[33] M. Benning, L.F. Gladden, D.J. Holland, C.-B. Schönlieb, T. Valkonen, Phase reconstruction from velocity-encoded MRI measurements – a survey of sparsity-promoting variational approaches, J. Magn. Reson. 238 (2014) 26–43, http://dx.doi.org/10.1016/j.jmr.2013.10.003.

[34] B.M.A. Delattre, R.M. Heidemann, L.A. Crowe, J.-P. Vallée, J.-N. Hyacinthe, Spiral demystified, Magn. Reson. Imaging 28 (2010) 862–881, http://dx.doi.org/10.1016/j.mri.2010.03.036.

[35] A. Chambolle, P.-L. Lions, Image recovery via total variation minimization and related problems, Numer. Math. 76 (1997) 167–188.

[36] C.R. Müller, D.J. Holland, J.F. Davidson, J.S. Dennis, L.F. Gladden, A.N. Hayhurst, et al., Geometrical and hydrodynamical study of gas jets in packed and fluidized beds using magnetic resonance, Can. J. Chem. Eng. 87 (2009) 517–525, http://dx.doi.org/10.1002/cjce.20191.